Biomedical Optics EXPRESS

Adaptive optics two-photon excited fluorescence lifetime imaging ophthalmoscopy of photoreceptors and retinal pigment epithelium in the living non-human primate eye

SARAH WALTERS,[1,2,3,6] JAMES A. FEEKS,[1,2,3,6] KHANG T. HUYNH,[2,4] AND JENNIFER J. HUNTER[1,2,4,5,*]

[1] The Institute of Optics, University of Rochester, Rochester, NY 14642, USA
[2] Center for Visual Science, University of Rochester, Rochester, NY 14642, USA
[3] Currently with IDEX Health & Science, West Henrietta, NY 14586, USA
[4] Department of Biomedical Engineering, University of Rochester, Rochester, NY 14642, USA
[5] Flaum Eye Institute, University of Rochester, Rochester, NY 14642, USA
[6] These authors contributed equally
[*] jhunter@ur.rochester.edu

Abstract: Fluorescence lifetime imaging has demonstrated promise as a quantitative measure of cell health. Adaptive optics two-photon excited fluorescence (TPEF) ophthalmoscopy enables excitation of intrinsic retinal fluorophores involved in cellular metabolism and the visual cycle, providing *in vivo* visualization of retinal structure and function at the cellular scale. Combining these technologies revealed that macaque cones had a significantly longer mean TPEF lifetime than rods at 730 nm excitation. At 900 nm excitation, macaque photoreceptors had a significantly longer mean TPEF lifetime than the retinal pigment epithelium layer. AOFLIO can measure the fluorescence lifetime of intrinsic retinal fluorophores on a cellular scale, revealing differences in lifetime between retinal cell classes.

© 2021 Optica Publishing Group under the terms of the Optica Open Access Publishing Agreement

1. Introduction

In many retinal diseases, functional changes in retinal cell health occur before the onset of structural alterations visualized by clinical ophthalmic imaging. Thus, to allow for earlier detection of retinal disease, accelerate development of methods to restore vision, and continue advances in understanding of normal retinal function, it is essential to develop noninvasive, objective measures of retinal cell function. Two-photon excited fluorescence ophthalmoscopy (TPEFO) has demonstrated potential to provide such a measure in both healthy and diseased non-human primate eyes, as the kinetics of intrinsic two-photon excited fluorescence (TPEF) from photoreceptors are indicative of visual cycle activity and can be altered by interventions that impair photoreceptor function [1–3]. TPEFO has not only provided *in vivo* visualization and functional assessment of photoreceptors at the cellular scale, but the imaging modality has enabled improvements in endogenous structural contrast over that of conventional confocal reflectance imaging in several retinal layers, including the ganglion cell layer, inner and outer nuclear layers, and the retinal pigment epithelium (RPE) [4,5]. TPEFO takes advantage of the many molecules present in the retina that exhibit intrinsic fluorescence and can be excited by two photon absorption at near-infrared wavelengths, including collagen, elastin, reduced nicotinamide adenine dinucleotide (phosphate) (NAD(P)H), fully oxidized Flavin adenine dinucleotide (FAD), and retinoids (such as retinol, retinyl esters, A2E), and other components of RPE lipofuscin. NAD(P)H, FAD, and retinoids all play a critical role in processes essential to retinal function. NAD(P)H and FAD, present in all cells, are cofactors in oxidation-reduction reactions necessary for retinal metabolic

#444550 https://doi.org/10.1364/BOE.444550
Journal © 2022 Received 30 Sep 2021; revised 2 Dec 2021; accepted 2 Dec 2021; published 17 Dec 2021

Biomedical Optics EXPRESS

activity. Retinoids, found in the photoreceptors and RPE, are vital components of the visual cycle, which regenerates visual pigment in order to maintain photoreceptor function.

Although intensity-based TPEFO in non-human primate has successfully visualized several classes of retinal structures and probed both rod and cone function [1,4], fluorescence lifetime imaging at the cellular scale has the potential to provide further insight into both basic physiology and pathology of the retina. Characterizing the fluorescence lifetime, a measure of the duration a fluorescent molecule remains in its excited state, has several advantages compared to intensity-based fluorescence imaging. The lifetime of fluorescence is sensitive to the microenvironment of the fluorescent molecule, and can be unique for each fluorophore (6). Unlike intensity-based imaging, it is impervious to variations in excitation efficiency, emission intensity, absorption properties, and fluorophore concentration [6]. This is of particular importance when imaging the outer retinal layers, which require passage of both excitation and emission through several layers of vasculature and inner retina cell classes. *In vivo* single-photon widefield fluorescence lifetime imaging ophthalmoscopy (FLIO) has already been performed in the rodent and human fundus using a scanning laser ophthalmoscope [7,8]. Widefield FLIO has demonstrated promise as a quantitative measure of retinal health, prior to the appearance of structural changes [9]. Retinal fluorescence lifetime is altered in many retinal diseases, including age-related macular degeneration [10–15], retinitis pigmentosa [16,17], diabetic retinopathy [18], Stargardt disease [19,20], and choroideremia [21], among others [22–26].

We developed adaptive optics fluorescence lifetime imaging ophthalmoscopy (AOFLIO) to obtain cellular-scale fluorescence lifetime images from the living eye. By making lifetime measurements of TPEF obtained with an adaptive optics scanning light ophthalmoscope (AOSLO) we previously measured exogenous fluorescent markers in the mouse retina [27]. AOFLIO performed using TPEFO has two distinct advantages over single photon widefield FLIO. First, it enables resolution of fluorescence lifetime in individual cells. Second, use of nonlinear excitation enables access to the aforementioned fluorophores, which are efficiently excited only in the ultraviolet. Here, we demonstrate AOFLIO of TPEF in the living macaque and explore its potential to differentiate retinal cell classes, namely the photoreceptors and RPE.

2. Methods

2.1. Animal preparation

A total of four macaque monkeys (*Macaca fascicularis*), three males and one female ranging in age from 4-10 years old, were used in this study. Animals were handled according to protocols approved by the University of Rochester's Committee for Animal Research. Macaques were anesthetized with ketamine (10-20 mg/kg) and midazolam (0.25 mg/kg) and secured looking forward in a stereotaxic device in ventral recumbency. After intubation, anesthesia was maintained by inhalation of isoflurane (1-5%). To reduce eye movements, paralysis was induced with vecuronium (40-80 μg/kg/hour) or rocuronium (200-400 μg/kg/hour) for up to a 6-hour period. During paralysis, respiration was maintained by a ventilator. Mydriasis and cycloplegia were induced with 1 to 2 drops each of phenylephrine hydrochloride (2.5%) and tropicamide (1%). A rigid gas permeable contact lens (Oxyflow QC in Paragon PP02 Clear, ABB Optical Group), coated with Genteal (Alcon, Fort Worth, TX, USA), was placed on the cornea to maintain hydration and correct base refractive error. The eye was held open with a lid speculum, and the animal's pupil was aligned to the exit pupil of the AOSLO.

2.2. Imaging system and image acquisition

A custom AOSLO designed for excitation and collection of TPEF from the living non-human primate retina was modified for TPEF AOFLIO. The AOSLO has been previously described in detail with a system diagram [1]. Briefly, a laser diode (840 nm, 40 μW; QPhotonics, Ann Arbor,

Biomedical Optics EXPRESS

MI, USA) used for wavefront sensing, a super luminescent diode (790 nm, 200 μW; Superlum, Cork, Ireland) used for reflectance imaging, and a tunable ultrashort pulsed Ti:Sapphire laser (tuned to 730 or 900 nm, 7 mW, ~55 fs pulse duration, 80 MHz repetition rate; Mai Tai XF-1; Newport Spectra-Physics, Santa Clara, CA, USA) used for excitation of TPEF were raster scanned on the retina. For the TPEF source, low-order dispersion of the system and eye were compensated (DeepSee, Newport Spectra-Physics) to maximize the *in vivo* collection of emitted fluorescence photons. A deformable mirror in combination with a Hartmann-Shack wavefront sensor were used to correct and measure the optical aberrations, respectively. Light levels noted represent the average power of a 7.5 mm diameter beam incident on the cornea. Light reflected from the retina and passing through the pupil of the eye was descanned through the system and collected to reconstruct reflectance images. TPEF emission was collected <600 nm at 730 nm excitation and <680 nm at 900 nm excitation without descanning by a hybrid photon counting detector (HPM-100-40; Becker and Hickl, Berlin, Germany). Images were captured with a rectangular field of view ranging from 0.73° x 0.84° to 2.0° x 2.2°. Two monkeys were imaged with both 730 nm and 900 nm excitation. One monkey was only imaged with 730 nm excitation. Another was only imaged with 900 nm excitation. At 730 nm excitation, photoreceptors were imaged in 19 locations across 3 monkeys from 2° to 22° eccentricity. At 900 nm excitation, both photoreceptors and RPE were imaged in 24 locations across 3 monkeys from 2° to 20° eccentricity.

Due to the cardiac cycle and respiration of the animal, motion occurred between frames. An image-based tracking algorithm operating in closed loop was used to optically stabilize the image in real time by manipulating a two-axis fast steering mirror (S-334.2SL; Physik Instrumente, Karlsruhe, Germany) [28]. The algorithm used the 790 nm reflectance video focused at the photoreceptor layer as a tracking signal. Residual motion is expected to have a maximum root-mean-square less than 0.5 arcmin. This may lead to small, occasional inaccuracies in the pixel assignment of photons.

For photoreceptor imaging, the 790 nm source and Ti:Sapphire laser were co-focused at the photoreceptor layer. For RPE imaging, the 790 nm source was focused at the photoreceptor layer to maintain a high signal-to-noise ratio (SNR) stabilization signal, while the Ti:Sapphire laser was focused more sclerad to excite TPEF from the RPE. This dual-focus method individually adjusts the vergence of each source entering the system, relative to the wavefront sensing source and is described in detail elsewhere [29]. Real-time optical stabilization enabled TPEF lifetime data to be averaged over many frames without post-registration.

TPEF lifetime data was acquired using a time-correlated single photon counting (TCSPC) module (SPC-160; Becker and Hickl GmbH, Berlin, Germany). A fast photodiode (PHD-400; Becker and Hickl GmbH) captured the pulses of the Ti:Sapphire laser and was used as the synchronization signal for the TCSPC module. Collected TPEF photons were assigned to one of 256 time bins for each pixel, depending on arrival time with respect to the synchronization pulse. Images were acquired over 120 to 150 seconds with resolution of 250 by 300 pixels using the acquisition software provided with the TCSPC module (SPCM; Becker and Hickl GmbH). A TPEF intensity image was generated by summation of all photons captured at a pixel. Unlike the reflectance images, which were acquired using custom software, these images were unable to be desinusoided.

2.3. Lifetime image analysis

TPEF lifetime data at each pixel was fit to a double exponential decay model in the image analysis software provided with the TCSPC module (SPCImage; Becker and Hickl GmbH), using a binning factor of 2, which binned 5×5 pixels around each fitted pixel to increase the SNR of calculated lifetimes. The fits were generated using the equation

$$I(t) \propto \; a_1 exp^{-\frac{t}{\tau_1}} + a_2 exp^{-\frac{t}{\tau_2}} \tag{1}$$

Biomedical Optics EXPRESS

where $I(t)$ is the TPEF intensity at time t after the excitation pulse, a_1 and a_2 are the contributions of the fast and slow lifetimes, and τ_1 and τ_2 are the corresponding fast and slow lifetimes. The mean TPEF lifetime, τ_m, was defined as $\tau_m = a_1\tau_1 + a_2\tau_2$, where $a_1 + a_2 = 1$. Mean fluorescence lifetime images were generated using the color gradient typical of traditional fluorescence lifetime data in microscopy (red long, blue short) rather than the opposite, which is used for widefield FLIO.

The quality of the fit was determined using ${\chi_R}^2$, a measure of the goodness of fit in which a value closer to unity represents a better fit to the data [30]. To ensure sufficient SNR, a threshold of 100 photons in the time channel with maximum signal at each pixel after spatial binning was used. This threshold was achieved at all pixels with the exception of those underlying large retinal vessels. Using TCSPC and this analysis procedure, contributions from fluorophores with fluorescence lifetimes longer than 50 ps can be detected [31]. Shorter lifetime components may be present but will not be detected.

2.4. Phasor analysis

In addition to analysis using exponential decays, phasor plots [32,33] of each image were generated using custom software developed in MATLAB (MathWorks, Inc. Natick, MA, USA). The Fourier transform of the decay curve at each pixel in the image, deconvolved with the instrument response function (IRF) automatically generated in SPCImage, was taken and evaluated at the laser repetition angular frequency (2π * 80 MHz). The auto IRF is calculated from the rising edge of the decay histogram in an area surrounding the brightest region of the image. For each pixel, this produced a single complex number, or phasor, whose real (g) and imaginary (s) components can be plotted as a coordinate pair (g,s) on a semicircular plot. Specifically, these components are:

$$g_{p,q} = \frac{\sum_{t=0}^{N_{bins}} d_{p,q}[t]\cos(\mathrm{t} * 2\pi * 80MHz)}{\sum_{t=0}^{N_{bins}} d_{p,q}[t]} \tag{2}$$

$$g_{p,q} = \frac{\sum_{t=0}^{N_{bins}} d_{p,q}[t]\sin(\mathrm{t} * 2\pi * 80MHz)}{\sum_{t=0}^{N_{bins}} d_{p,q}[t]} \tag{3}$$

where $d_{p,q}[t]$ is the recorded photon decay histogram at pixel (p, q), t is the time bin, and N_{bins} is the total number of time bins. Pixels whose corresponding phasors lie on the semicircle have a one-component exponential decay; those within the semicircle are comprised of a linear combination of two or more lifetime components. Phasors representing longer lifetimes lie closer to the origin.

2.5. Analysis of cone and rod lifetimes

For photoreceptor images at 730 nm excitation, exponential fit parameters were analyzed separately for cones and rods. Masking of the images was manually performed using custom software. The TPEF intensity image was used to identify cones, which were individually masked by marking the perimeter of each cone with a user-adjustable ellipse. The axes of the ellipses were then decreased by a factor of 0.2 to minimize crosstalk between cone and rod pixels resulting from binning. This partially compensated for any small errors in the pixel assignment of individual photons resulting from inaccuracies in optical stabilization. Cone lifetime fit parameters were output for each pixel within the cone mask. For analysis of rod-populated regions the original cone mask was inverted and expanded by a factor of 0.2, and lifetime fit parameters were output for each pixel within the inverted mask. A factor of 0.2 was found to be the optimal value for shrinking or expanding the mask in order to analyze the maximum amount of cone or rod pixels while reducing crosstalk caused by binning. For each image location, all cone pixels were averaged to determine each lifetime parameter for cones, and analogously for rods. Although

Biomedical Optics EXPRESS

cones were masked for all eccentricities, rod data was not analyzed for eccentricities less than 5°, as rod density was too low to warrant analysis with sufficient signal-to-noise-ratio.

For analysis of data collected at 730 nm excitation, all fit parameters (a_1, τ_1, τ_2, and τ_m) were analyzed for rods and cones separately. For analysis of data collected at 900 nm, all fit parameters were analyzed by averaging across all pixels in each image. The fit parameter a_2 was not included in any analysis, as the contributions of the fast and slow lifetimes were constrained by $a_1 + a_2 = 1$.

2.6. Statistical analysis

Statistical differences were determined using a multi-way analysis of variance (ANOVA) performed in either MATLAB or SPSS (IBM Corp., Armonk, NY, USA) to determine significance between animals, eccentricities, and cell class (i.e. cones or rods in the case of 730 nm excitation and photoreceptors or RPE in the case of 900 nm excitation). A p-value of less than 0.05 was used as the threshold for significance.

2.7. Lifetime imaging in regions of photodamage

To demonstrate the potential of AOFLIO to identify variations in abnormal retinal regions we assessed a different example of photodamage for each excitation wavelength. AOFLIO was performed in two of the monkeys that each had one retinal location exposed to damaging levels of light at least 1 month prior to imaging. Photodamage location 1 was assessed in the photoreceptor layer with AOFLIO of TPEF at 730 nm excitation. Photodamage had occurred as a result of exposure in a 0.5° square field of view to 34 J/cm^2 of 460 nm CW laser light as part of a study to determine photochemical light damage thresholds across the visible spectrum in macaque. Assessment across a 2° square field of view with AOSLO reflectance and single-photon visible fluorescence imaging showed that this exposure caused disruption to both the photoreceptor and RPE mosaics [34]. Photodamage location 2 was assessed in only the RPE layer with AOFLIO of TPEF at 900 nm excitation. Photodamage had been caused by an acute exposure to over 100 mW of femtosecond pulsed 730 nm laser light (~400 J/cm^2), completely ablating the photoreceptor layer and damaging the RPE as observed with AOSLO reflectance imaging. Reflectance images and records of the initial exposure locations were used to accurately identify and image with AOFLIO the corresponding locations. Widefield images (Spectralis HRA + OCT; Heidelberg Engineering, Heidelberg, Germany) of the vasculature provided maps used to navigate the retina to the specific regions of interest. Because of the small number of samples, no statistical analyses were performed on this exemplary data.

2.8. Ex vivo retina preparation and imaging

A microscope arm was added to the existing non-human primate AOSLO to allow for TPEF lifetime imaging of *ex vivo* macaque retina (see Appendix). These were not the same macaques used for the *in vivo* imaging studies. The AOSLO exit pupil was magnified and matched with a water immersion objective (W Plan-Apochromat 20X/1.0; Zeiss, Oberkochen, Germany). At the time of sacrifice, macaque retinas were either fixed or left unfixed. For fixation, animals were perfused with 1L of heparinized 0.9% saline followed by 2L 4% paraformaldehyde. In both cases, eyes were enucleated and anterior optics discarded. Fixed tissue was immersed in 4% paraformaldehyde overnight. Retinal dissection was performed under white light with the retina/RPE left intact. Unfixed tissue was maintained in modified Mammalian Ringer's solution with a composition in mM: 130 NaCl, 5 KCl, 0.5 $MgCl_2$, 2 $CaCl_2$, 25 HEPES, 5 glucose, pH = 7.40, Osmolality = 310 mOsm at 37°C [35]. For imaging both fixed and unfixed tissue, small pieces of the retina/RPE complex were dissected and immersed in modified Mammalian Ringer's solution. The photoreceptor layer of both fixed and unfixed retina was imaged *en face* at 730 nm excitation. Unfixed macaque retina was imaged between 1.5 to 3 hours after time of

Biomedical Optics EXPRESS

sacrifice. Collection and analysis of TPEF lifetime data was performed as described for *in vivo* data.

3. Results

3.1. Lifetime imaging of photoreceptors at 730 nm excitation: cones have a longer mean lifetime than rods

At every retinal eccentricity imaged, cones were visually distinguishable in the 730 nm excitation TPEF mean lifetime image. The longer lifetimes of the cones provided contrast from surrounding rods (Fig. 1(a) and 1(b)). The difference in mean lifetime was corroborated by phasor analysis, which produced a distribution of phasor coordinates from each pixel in the photoreceptor image in which all phasor coordinates laid on a single linear trajectory within the phasor semicircle (Fig. 1(c)). Phasor coordinates corresponding to cone pixels laid on the left side of the linear trajectory closer to the origin, which were representative of a longer fluorescence lifetime. Coordinates corresponding to rod pixels laid on the right side of the trajectory closer to (1,0), representative of a shorter fluorescence lifetime (Fig. 1(d)).

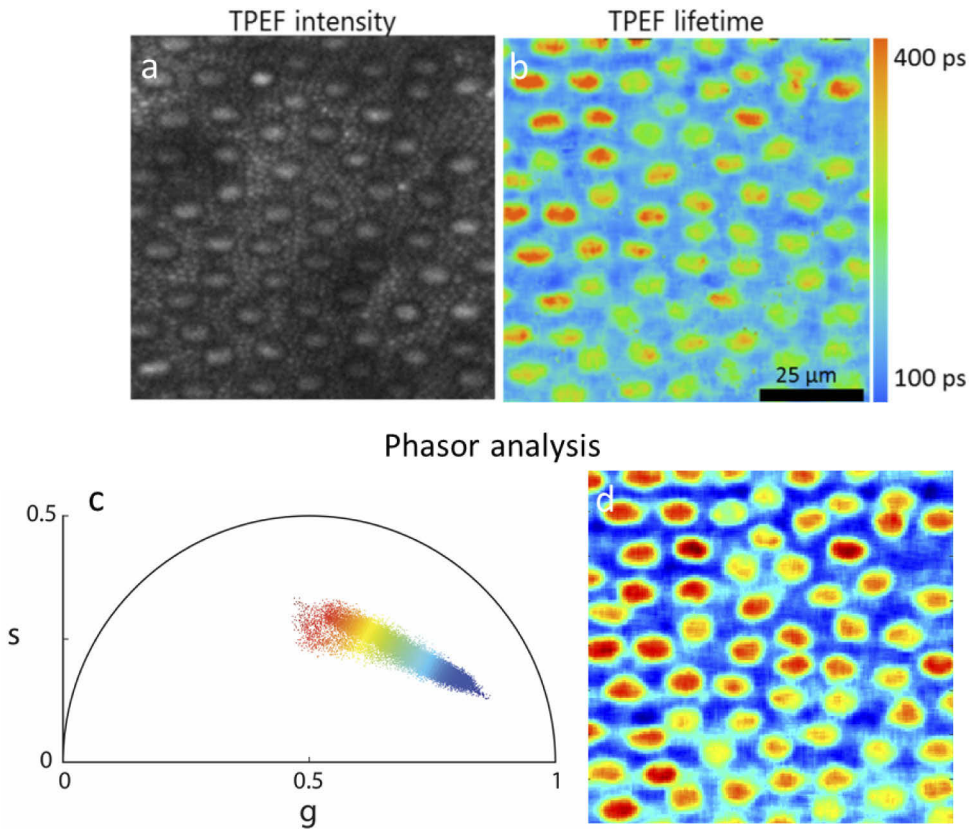

Fig. 1. AOFLIO images at 730 nm excitation of TPEF intensity (a) and mean TPEF lifetime (b) of the photoreceptors at ~20° eccentricity. Cones can be distinguished from rods by their longer lifetime. A phasor plot from the same image is shown in (c), where a color applied to each point on the phasor plot corresponds to pixels in (d). Cones can be distinguished from rods in this case by their phasor coordinates.

Biomedical Optics EXPRESS

An ANOVA was performed for all data collected at 730 nm excitation to assess for variations within and interaction effects between three factors (monkey, eccentricity, photoreceptor type). For all fluorescence lifetime parameters (τ_m, τ_1, τ_2, a_1), no significant interactions were found.

To assess variations between monkeys, data was averaged across all eccentricities. Across the three monkeys in which this data was collected, no significant difference was found in any of the lifetime parameters (τ_m, τ_1, τ_2, a_1, $p > 0.05$). Data were averaged across the 3 monkeys for the remainder of the analysis performed at 730 nm. Across all imaging locations, cones had a significantly longer mean lifetime than rods (τ_m, $p < 0.01$). This was a result of cones having both a longer fast (τ_1, $p < 0.01$) and slow (τ_2, $p < 0.01$) lifetime component in addition to a smaller contribution of the fast lifetime component than rods (a_1, $p < 0.01$). Values of lifetime parameters for rods and cones across all imaging locations (n = 19 locations, mean determined across monkeys and eccentricities) are summarized in Table 1.

Table 1. TPEF lifetime parameters of cones and rods. Cones exhibit longer τ_1 and τ_2, while rods have a higher a_1. Together, these parameters drive a difference in the mean lifetime τ_m, which is longer for cones than it is for rods.

Photoreceptor	τ_1 (ps)	τ_2 (ps)	a_1	τ_m (ps)
Cones	129 ± 3	2060 ± 20	92.8 ± 0.4	265 ± 11
Rods	114 ± 4	1880 ± 20	95.4 ± 0.3	195 ± 9

3.2. *Lifetime imaging of photoreceptors at 730 nm excitation: cone and rod mean lifetimes shorten with eccentricity*

Averaging across 3 monkeys, the mean fluorescence lifetime of both photoreceptor types was found to shorten significantly as eccentricity increased ($p < 0.01$), with the most pronounced shortening occurring from 2° to 5° (Fig. 2(a)). There was still a significant difference in mean lifetime with eccentricity even if data from an eccentricity of 5° or less was excluded from the analysis (τ_m, $p = 0.01$). No significant differences with eccentricity were found in the fast (τ_1, $p = 0.05$) or slow (τ_2, $p = 0.64$) lifetimes. However, the amplitude of the fast lifetime component increased with eccentricity (Fig. 2(b)); a_1, $p < 0.01$), with the most pronounced increase occurring from 2° to 5°. This concurrent rise in contribution of the fast lifetime component, coupled with no significant changes in the fast or slow lifetimes, suggest that the change in rod and cone mean lifetime with eccentricity is primarily driven by a change in the contribution of the fast and slow lifetime components, not the lifetimes themselves.

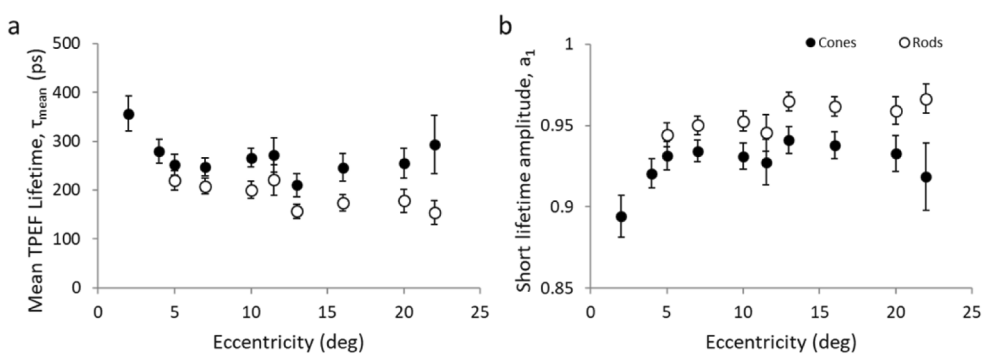

Fig. 2. (a) Mean TPEF lifetime $\boldsymbol{\tau}_m$ and (b) slow lifetime amplitude a_1 both vary as a function of eccentricity. $\boldsymbol{\tau}_m$ shortens significantly and a_1 increases significantly. In addition, it can be seen that the cone lifetime is longer than that of the rods at all eccentricities. Error bars indicate the standard error of all data acquired for each eccentricity.

Biomedical Optics EXPRESS

3.3. Lifetime imaging of photoreceptors at 730 nm excitation: photoreceptor lifetime altered in regions of photodamage

Photoreceptors were imaged in a region of exposure to a damaging light level, resulting in retinal photodamage. In photodamage location 1 (34 J/cm^2 at 460 nm), the photoreceptor mosaic was disrupted (Fig. 3(a)). It is expected that the RPE mosaic is also disrupted at this location [36]. Masking of the rods and cones was performed for this location. For rods and cones, mean lifetime parameters within the damaged region (Fig. 3(b)) were averaged and compared to the surrounding region of normal appearing photoreceptors. The mean fluorescence lifetimes of cones and rods were reduced when compared to normal regions in the surrounding tissue (Fig. 3(c)). The phasor plot indicated a small shift in the mean g coordinate and a change in shape of the phasor cluster (Fig. 3(d)).

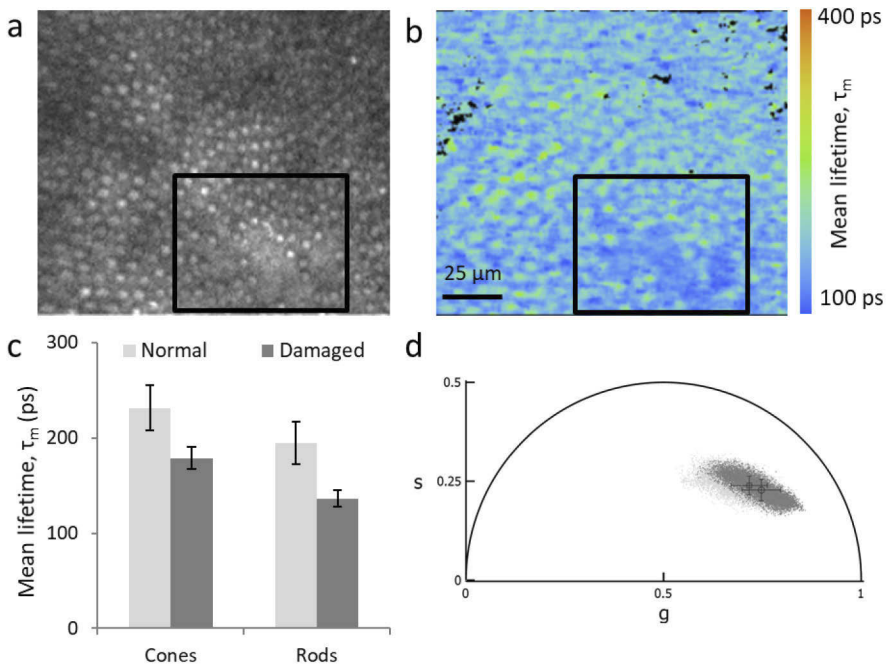

Fig. 3. TPEF intensity (a) and mean lifetime (b) images of a photodamaged region. The region of light exposure was contained within the outlined area. Photodamage location 1 was exposed to 34 J/cm^2 of 460 nm light. (c) The average τ_m of cones and rods in both the damaged region and the surrounding control region. The measured lifetime in rods and cones appears to be reduced in the region of photodamage. Error bars indicate the standard deviation of the mean lifetime across masked pixels in each region. Corresponding phasor plots (d) also indicate small differences between the normal (light gray, center of mass denoted by square) and damaged (dark gray, center of mass denoted by circle) retinal locations.

3.4. Lifetime imaging of photoreceptors at 730 nm excitation: cones and rods have different mean lifetime in unfixed but not fixed tissue

For comparison to lifetimes collected *in vivo*, AOFLIO was performed *ex vivo* in the photoreceptor layer in both fixed and fresh, unfixed excised macaque retina. Images from fresh, unfixed photoreceptor layer demonstrated a difference in rod and cone mean lifetime, similar to observations *in vivo* (Fig. 4(a) and 4(b)). However, fixed photoreceptors did not show a difference between rod and cone mean lifetime (Fig. 4(c) and 4(d)). In both cases, mean TPEF lifetime of the

Biomedical Optics EXPRESS

photoreceptor layer *ex vivo* was much longer than *in vivo*, ranging from approximately 300 to 900 ps (Fig. 4(b) and 4(d)). Cones and rods exhibited mean lifetimes of 800 ± 80 ps and 560 ± 110 ps, respectively, in fresh, unfixed retina, over 300 ps longer compared to mean lifetimes of *in vivo* cones and rods (Table 1).

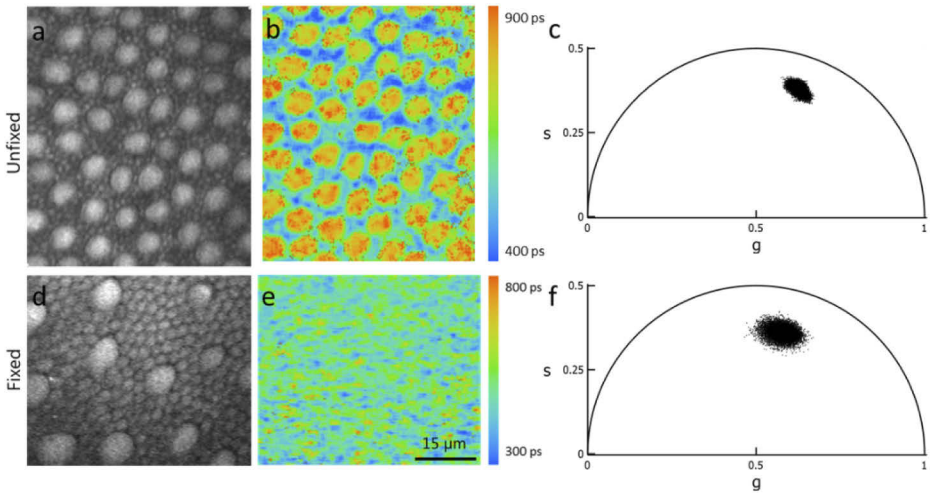

Fig. 4. TPEF intensity (a,d) and corresponding mean lifetime (b,e) and phasor plots (c,f) of photoreceptors in the macaque retina in unfixed (a,b,c) and fixed (d,e,f) conditions with 730 nm excitation. Cones and rods are distinguishable when tissue is unfixed, but not when tissue is fixed.

3.5. Lifetime imaging of photoreceptors and retinal pigment epithelium at 900 nm excitation: photoreceptor and RPE lifetimes are uniform across imaging field

Though structure of photoreceptors and RPE was visible in the TPEF intensity images at 900 nm excitation (Fig. 5(a) and 5(d)), mean lifetime was relatively uniform across the imaging field for both (Fig. 5(b) and 5(e)). Phasor plots corroborated this observation with a tight clustering of points near the semicircle at a similar locus for both photoreceptors and RPE (Fig. 5(c) and 5(f)). This cluster of phasor points near the semicircle suggests dominance of a singular fluorescent species for both the photoreceptors and RPE with a relatively short mean lifetime.

For each retinal layer (photoreceptors and RPE), a total of 24 locations were imaged evenly distributed across 3 monkeys. Across all imaging locations (3 monkeys across different eccentricities), photoreceptors had a significantly longer mean lifetime than RPE (τ_m, $p < 0.01$). This was a result of photoreceptors having longer fast (τ_1, $p < 0.001$) and slow (τ_2, $p < 0.001$) lifetime components than RPE despite a larger contribution of the fast lifetime component (a_1, $p < 0.001$). Lifetime parameters were found to be significantly different across the three monkeys imaged (τ_m, τ_1, a_1, $p < 0.01$), with the exception of the slow lifetime (τ_2, $p = 0.07$). For this reason, data is presented for each monkey individually. Values of lifetime parameters for photoreceptors and RPE at all imaging locations are summarized in Table 2.

3.6. Lifetime imaging of photoreceptors and retinal pigment epithelium at 900 nm excitation: photoreceptor and RPE lifetimes vary with eccentricity

The mean fluorescence lifetime was found to vary with eccentricity for both photoreceptors and RPE (τ_m, $p < 0.05$), although with different trends. For statistical analysis, data across 3 monkeys was considered without an interaction. Photoreceptor mean lifetime shortened monotonically

Biomedical Optics EXPRESS

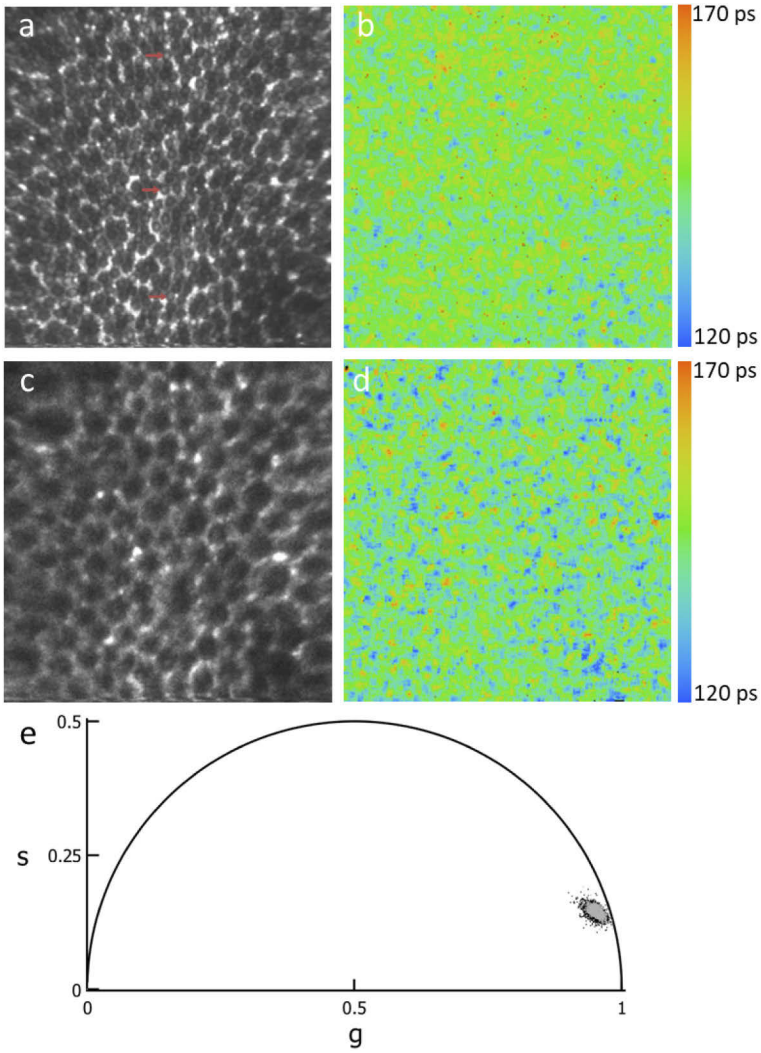

Fig. 5. TPEF intensity (a,c) and mean lifetime (b,d) images at 900 nm excitation of photoreceptors (a,b) and RPE (c,d) at ~8° eccentricity. Red arrows denote examples of individual cones in the fluorescence intensity image. No analogous structure is observed in the mean fluorescence lifetime images. Corresponding phasor plots for the photoreceptor layer (gray) and the RPE layer (black) are overlapping and shown in (e). The phasor plots show a tight cluster of pixels, pointing towards a uniform mean lifetime throughout the imaging field.

further into the periphery, whereas RPE lifetime became more prolonged until approximately 13°, at which point it began to shorten (Fig. 6). The shortening in mean lifetime of photoreceptors was primarily caused by a shortening in both the fast and slow lifetime components (τ_1, τ_2, $p < 0.001$); however, the lifetime contributions were also changed with eccentricity (a_1, $p < 0.05$). In the case of RPE, the change in mean lifetime was a consequence of both a change in fast lifetime (τ_1, $p < 0.05$) and its contribution (a_1, $p < 0.05$). The slow lifetime was not found to vary significantly with eccentricity (τ_2, $p = 0.14$).

Biomedical Optics EXPRESS

Table 2. TPEF lifetime parameters of photoreceptors and RPE at 900 nm excitation. Photoreceptors exhibit a slightly longer mean lifetime than the RPE in each monkey, though the absolute lifetime values are significantly different across monkeys. Fluorescent lifetimes were longer for both photoreceptors and RPE with increased age.

Monkey	Layer	τ_1 (ps)	τ_2 (ps)	a_1	τ_m (ps)
Monkey 1 (5 y.o.)	Photoreceptors	118 ± 2	810 ± 40	95.9 ± 0.15	142 ± 2
	RPE	110 ± 3	630 ± 10	94.4 ± 0.14	138 ± 1.9
Monkey 2 (7 y.o.)	Photoreceptors	121 ± 3	770 ± 40	95.5 ± 0.15	147 ± 3
	RPE	112 ± 1.5	610 ± 10	93.6 ± 0.18	140 ± 1.4
Monkey 3 (10 y.o.)	Photoreceptors	127 ± 1.0	820 ± 20	95.7 ± 0.16	156 ± 1.7
	RPE	121 ± 1.9	680 ± 10	94.5 ± 0.15	149 ± 1.7

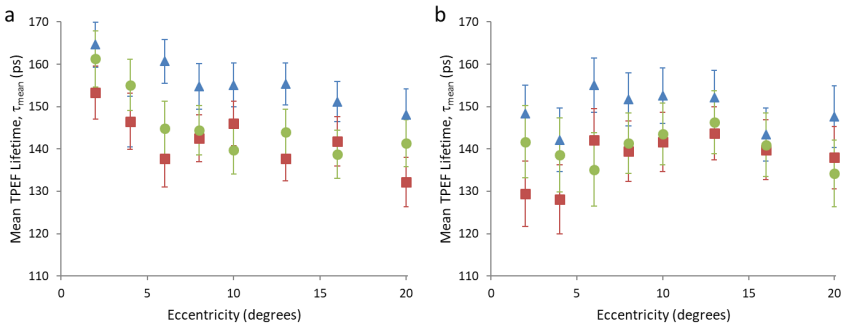

Fig. 6. TPEF mean lifetime of photoreceptors (a) and RPE (b) at 900 nm excitation at eccentricities from 2° to 20°. Photoreceptor lifetime shortens over the eccentricities measured. RPE lifetime prolongs, peaks around 13°, and then shortens. Data is shown separately for each macaque (monkey 1, green circles; monkey 2, red squares; monkey 3, blue triangles).

3.7. Lifetime imaging of photoreceptors and retinal pigment epithelium at 900 nm excitation: RPE lifetime altered in region of photoreceptor ablation

AOFLIO was performed at 900 nm excitation in photodamage location 2 which had been previously exposed to a high level (> 100 mW) of pulsed, near-infrared light, ablating the

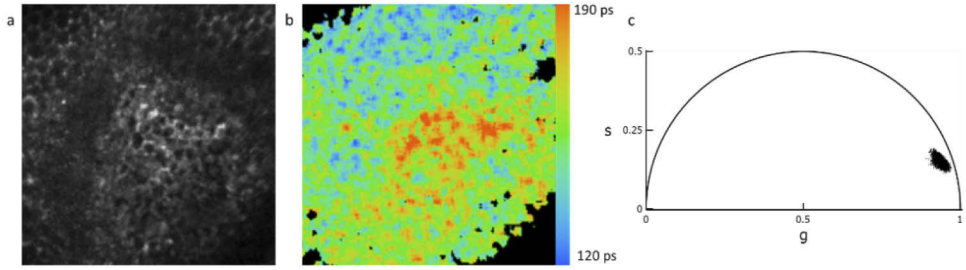

Fig. 7. AOFLIO at 900 nm excitation in photodamage location 2 (>100 mW of 730 nm light from a fs-pulsed laser). TPEF intensity (a) and corresponding mean lifetime (b) and phasor plot (c) of RPE. Mean lifetime is prolonged in the damaged region when compared to surrounding RPE. Black regions indicate an insufficient number of photons for exponential fitting.

Biomedical Optics EXPRESS

photoreceptors and causing damage to the RPE (Fig. 7(a)). The RPE within the damaging exposure exhibited a longer mean TPEF lifetime (168 ± 12 ps) than the surrounding unexposed RPE (149 ± 10 ps) (Fig. 7(b)).

4. Discussion

Here, we present the first *in vivo* AOFLIO of intrinsic TPEF on a cellular scale in the non-human primate retina. The transverse (~2 µm) and axial (~30 µm reflectance, ~25-50 µm TPEF [4]) resolution achievable with an AOSLO enables ascription of TPEF lifetime measurements to particular cell classes, which we demonstrate to be differentiable by AOFLIO. Though absolute fluorescence lifetimes are reported here, interpretation of lifetime values can prove challenging. In the present study, we have limited our analysis to a double exponential fit. However, it is probable more than two fluorescent species contribute to the fluorescence signal in the retina, even if the contributions are small. Furthermore, exponential fitting algorithms can have a substantial impact on the reported fluorescence lifetime, making it difficult to compare absolute lifetimes across acquisition schemes and analysis paradigms. In addition, there is a scarcity of knowledge of the lifetime of fluorophores in the living retina. Because their environment as well as enzyme binding affect the fluorescence lifetime of many molecules, it can be challenging to extrapolate lifetime values from the studies, which established fluorescence lifetimes of many of these molecules in solution [37–39]. A summary of mean lifetimes of expected retinal fluorophores, as well as measurements of the lifetime in various retinal tissue preparations, is provided in Table 3.

Although measurements of the fluorescence lifetime in *ex vivo* retina have been made [40–43], it is not a direct replacement for *in vivo* fluorescence lifetime measurements. We found that mean 730 nm excited TPEF lifetime differences were maintained between rods and cones in fresh, *ex vivo* tissue, but not in fixed tissue. However, it was noted that lifetimes were lengthened in both unfixed and fixed *ex vivo* preparations relative to *in vivo* measurements. This is a probable result of underlying alterations in functional processes, and thus TPEF contributions and/or lifetimes, stemming from the removal of the retina/RPE complex from its native environment. Predicting the source of the *ex vivo* shift in fluorescence lifetime is challenging as many changes take place in the retina post-mortem. For example, NADH levels drop quickly in isolated tissue, likely reducing their contribution to the *ex vivo* signal in comparison to their contribution *in vivo* [44,45]. Although the fluorescence from NADH (free or bound) has a lifetime longer than our measured mean fluorescence lifetime, it is much shorter than the long lifetime component (τ_2~2000 ps). Loss of NADH may result in a shift of the relative contributions from the fluorophores within the photoreceptor layer. In addition, exposure to light during sample preparation may increase levels of retinol, known to have a much longer fluorescence lifetime (3000-3900 ps). Further difficulties stem from known effects of viscosity, which can prolong lifetime values in fixed tissue, and the effect of excitation wavelength on the lifetime of complex fluorophores such as those in RPE lipofuscin [38]. Nevertheless, the TPEF lifetime range in both the fixed and unfixed macaque photoreceptor layer was in good agreement with TPEF lifetime measurements in *ex vivo* porcine photoreceptors at 760 nm excitation (~300–900 ps) [42]. These challenges highlight the need for *in vivo* fluorescence lifetime imaging on a cellular scale, but also underscore the challenges in interpreting *in vivo* fluorescence lifetime data.

At 730 nm excitation, TPEF originating from cones had a significantly longer mean lifetime than TPEF from rods. Rods and cones are known to be both morphologically and functionally different. As such, fluorescence lifetime is influenced by a number of factors which may be different for rods and cones. One likely possibility is that there is a difference in relative TPEF contribution between the two photoreceptor types, such as from all-*trans*-retinol, NADH, or FAD, which are all efficiently excited at 730 nm and have emission within the bandwidth captured by our detector [46,47]. Our previous work identified the dominant time-varying fluorophore in

Table 3. Summary of mean fluorescence lifetimes of expected retinal fluorophores and various retinal tissue preparations.

Signal Source	Species	λ_{ex} (nm)	λ_{em} (nm)	Preparation	τ_m (ns)	Reference
NADH (free)	-	740	350-550	-	0.4	Vishwasrao, Heikal et al. 2005 [50]
NADH (bound)				mMDH bound	0.8	
FAD (free)	-	355	-	-	2.3	Nakashima, Yoshihara et al. 1980 [54]
FAD (bound)				DAAO bound	0.04 - 0.13	
Retinol	-	-	-	Various solutions	3.0 - 3.9	Chihara, Takemura et al. 1979 [37]
Carotenoids (lutein and zeaxanthin)	-	473	498-560	Various solutions	0.04–0.09	Sauer, Anderson et al. 2018 [69]
A2E	-	446	510-700	-	0.2	Schweitzer, Schenke et al. 2007 [62]
	-	413	450-600	DMSO solution	2.6	Cubeddu, Taroni et al. 1999 [40]
	-	485	556	-	4.0	Yakovleva, Feldman et al. 2017 [75]
Lipofuscin	-	446	510-700	-	1.4	Schweitzer, Schenke et al. 2007 [62]
	Human	364	-	Isolated	0.4 - 1.3	Docchio, Boulton et al. 1991 [66]
RPE Melanin	Human	364	-	Isolated	0.7 - 1.3	Docchio, Boulton et al. 1991 [66]
Melanosomes	Porcine	750	380-680	Isolated or *ex vivo*	0.1	Miura, Huettmann et al. 2013 [41]
RPE cell culture	Human	473	498-720	*In vitro*	1.2 - 1.7	Dysli, Berger et al. 2017 [24]
		413	450-600	*In vitro*	1.7	Cubeddu, Taroni et al. 1999 [40]
RPE	Murine	740-805	<600	*Ex vivo*, fresh	0.3 - 2.4	He, Ye et al. 2015 [76]
	Porcine	760	500-700	*Ex vivo*, fresh	0.07	Peters, Hammer et al. 2011 [42]
		446	510-700	*Ex vivo*	0.3	Schweitzer, Schenke et al. 2007 [62]
	Human	430	445-605	*Ex vivo*, fixed	0.4	Schweitzer, Gaillard et al. 2012 [43]
Photoreceptors	Porcine	760	500-700	*Ex vivo*, fresh	0.3 - 0.9	Peters, Hammer et al. 2011 [42]
Fundus	Human	473	498-720	*In vivo*	0.1 - 0.3	Dysli, Quellec et al. 2014 [8]
						Sauer, Schweitzer et al. 2015 [61]

Biomedical Optics EXPRESS

TPEFO of photoreceptors as retinol [2], consistent with *ex vivo* spectral measurements from outer segments in photoreceptors of frogs and mice [35]. However, pure all-*trans*-retinol has a fluorescence lifetime of 3–3.9 ns in various solvents [37], which is an order of magnitude greater than the mean lifetime reported here. This discrepancy may indicate that retinol is not a major contributing fluorophore or may be related to how the fluorescence lifetime is modified when retinol is free within the photoreceptor outer segment or bound to a protein such as interphotoreceptor retinoid binding protein, which facilitates transport of retinol from the outer segments to the retinal pigment epithelium [48]. Another prominent source of fluorescence in photoreceptors is mitochondrial NADH in the inner segments [35]. The fluorescence lifetime of NADH is known to depend on its conformation and binding state, with free NADH in solution having a lifetime of ~400 ps [49,50], while NADH bound to the mitochondrial enzyme malate dehydrogenase exhibits a lifetime of ~800 ps [50]. The known fluorescence lifetime of both NADH states is longer than the mean lifetime observed in our measurements. One possible explanation for the shorter observed lifetime could be a contribution from all-*trans*-retinal, another intermediate molecule in the visual cycle, which has an extremely short fluorescence lifetime in ethanol solution [51]. However, due to the low quantum yield of retinal ($\sim 1 \times 10^{-4}$), it is unlikely to be a major contributor to the TPEF lifetime observed here [4,52,53]. FAD, on the other hand, is known to have a fluorescence lifetime of 40-130 ps when protein-bound [54]. In all likelihood, all of these sources of fluorescence combine together in different proportions in rods and cones. Smaller variations in these factors may contribute to the range of mean lifetimes observed between individual cones (Fig. 1(b) and 1(d)). The measurement of fluorescence lifetimes, as determined with fitting of double exponentials, is limited in its ability to adequately separate out each contributing factor in such complex biological systems. Therefore, to identify specific sources of fluorescence, it may be necessary to combine fluorescence lifetime analysis, including phasor analysis, with measurement of emission spectra.

Rod and cone lifetime remained differentiable over the range of eccentricities measured in the present study. The mean 730 nm excited TPEF lifetime of both photoreceptor types was shown to shorten with eccentricity, driven by a change in the lifetime contributions, but not in the lifetimes themselves. These results would suggest rods and cones have different lifetime constituents as well as relative contribution of constituents. This is perhaps not surprising as the densities of rods and cones vary with eccentricity in the primate retina [55,56]. The rod to cone ratio increases over the eccentricities measured. In addition, both rods and cones are morphologically changed as a function of eccentricity; cone and rod inner segment diameters become larger [57] and cone outer segment length decreases [58]. As a consequence, photopigment density also varies with eccentricity [59]. Additionally, the photoreceptor to RPE ratio is known to change across eccentricity [60], and functional variations could result as a consequence. Therefore, it is not unreasonable that the contributions of TPEF constituents from photoreceptors are changed from fovea to periphery.

The TPEF lifetime measurements performed with 730 nm excitation cannot easily be compared with existing *in vivo* fluorescence lifetime measures obtained using fluorescence lifetime imaging ophthalmoscopy (FLIO). FLIO makes use of a modified clinical scanning laser ophthalmoscope and single photon excitation, typically at 473 nm, to obtain lifetime measurements in the fundus. At this wavelength, it is improbable that there is appreciable fluorescence from either NAD(P)H or retinol, which in contrast are excited very efficiently at the 730 nm single photon excitation equivalent of 365 nm [46,47]. However, our measurements at 900 nm excitation, which have an equivalent single photon excitation of 450 nm, are more comparable to previous measurements performed using FLIO. Nevertheless, the mean lifetimes reported in the current study were comparable to *in vivo* FLIO measurements of the normal human fundus, which were on the order of 100–400 ps [8,61].

Biomedical Optics EXPRESS

At 900 nm excitation, TPEF from the photoreceptor layer had a significantly longer mean lifetime than TPEF from RPE. This is consistent with observations in *ex vivo* porcine retina, where a longer fluorescence lifetime was found in the neural retina than in the RPE [62,63]. The most dominant fluorophores in the fundus are those found in RPE lipofuscin-containing organelles [64], which consist of several fluorescent components [65]. The reported mean fluorescence lifetime from RPE lipofuscin varies widely and has been stated to be anywhere from 0.4–1.3 ns [62,66]. Other potential fluorophores excited at this wavelength include FAD in both the photoreceptors and RPE, and melanin in the RPE. FAD would be in a similar environment in both photoreceptors and RPE and may explain the similarity of lifetimes observed in the phasor plots. RPE melanin is expected to have a lesser contribution than RPE lipofuscin fluorophores to the lifetimes reported here [67,68].

In FLIO, the shortest lifetimes were observed in the fovea with prolonged mean lifetime further into the periphery [7,8]. The mean 900 nm excited TPEF lifetime of the RPE was shorter at the fovea, prolonging until approximately 13°, then shortening further into the periphery. The shorter foveal lifetime in FLIO was attributed to macular pigment, which is autofluorescent and known to have a very short fluorescence lifetime [61,69,70]. However, given the expected axial resolution of the AOSLO is ~30 µm, we ascertain that TPEF from macular pigment is not largely influencing the lifetimes measured with AOFLIO in the photoreceptors and RPE. However, it cannot be ruled out that the macular pigment may have a screening effect on the visible TPEF, which could alter the lifetime in that region [71].

Alterations in mean TPEF lifetimes were detected in regions of photodamage in both photoreceptors and RPE. At 730 nm excitation, AOFLIO of photoreceptors that had been subject to long exposures of either visible or pulsed near infrared light, resulting in loss of some photoreceptors, showed slightly shortened mean TPEF lifetimes. Cells that experience a decrease in metabolic demand or a shift toward glycolysis have been shown to have a shortened fluorescence lifetime [9,50]. At 900 nm excitation, a significantly longer mean TPEF lifetime was observed in RPE within the region subjected to a brief, high-intensity pulsed near-infrared exposure. In porcine RPE explants, an intense visible laser exposure led to the formation of bright, punctate autofluorescence induced by oxidative stress, which exhibited a longer lifetime than the surrounding RPE autofluorescence [41]. However, nominal RPE fluorescence in that study was attributed to melanin, not lipofuscin and the precursors as is suspected here.

Though the possibility of AOFLIO has been demonstrated, challenges remain in the acquisition of fluorescence lifetime data using TPEF in the living non-human primate eye. As a result of eye motion, even with real-time optical stabilization, post-capture image registration is desired to avoid image blur and fluorescence lifetime data being assigned to the incorrect pixel. Additionally, we do not have the capability to correct for the sinusoidal scan motion of the resonant scanner in our fluorescence lifetime data acquisition. In the present study, cropping was required to confine images to the nearly linear central portion of the scan and reduce desinusoiding artifacts. Future improvements, including correction of the sinusoidal scan motion, will allow for a larger effective field of view by eliminating the need to crop images. In its current form in non-human primates, AOFLIO requires long acquisition times with exposures over the ANSI maximum permissible exposure in order to generate fluorescence lifetime images with high fidelity. At exposures similar to those used here, short wavelength cones can be damaged [72]; therefore, reducing the incident optical power and/or reducing exposure times [73] is critical for future translation into humans.

As discussed, a challenge remains in interpretation of fluorescence lifetimes reported here due to the limitations associated with exponential fitting. However, phasor analysis has emerged as a promising method to analyze lifetime data independent of the absolute lifetime. With 730 nm excitation, cones and rods lie on either end of the same linear trajectory that is fairly uniform in width, suggesting the presence of different proportions of the same fluorophores. Phasor analysis

Biomedical Optics EXPRESS

combined with phasor fingerprinting of known fluorophores in isolation may help identify the *in vivo* presence and contributions of possible fluorophores [33,74].

AOFLIO performed using TPEFO can measure the fluorescence lifetime of intrinsic retinal fluorophores on a cellular scale in the living macaque and can differentiate retinal cell classes based on fluorescence lifetime. In addition, AOFLIO has the potential to provide further insight into both basic physiology and pathology of the retina. First, the use of TPEF enables excitation of fluorophores that cannot be efficiently excited using single photon excitation through the pupil of the living eye, such as NAD(P)H and retinol, which are essential to cellular metabolism and visual cycle function. Secondly, use of an AOSLO results in an increase in lateral resolution and a reduction of focal volume, enabling attribution of fluorescence lifetimes *in vivo* on the single-cell level. Here, we have shown AOFLIO to provide a robust measure of fluorescence lifetime of macaque rods and cones, which did not differ across primates, which may allow for rapid, simultaneous photoreceptor identification and assessment of cell health. In addition, we have demonstrated alteration in lifetime in regions of retinal damage. AOFLIO has the potential to not only provide further insight into the basic physiology of the retina in animal models, and eventually humans, but also detect changes in retinal function at the cellular scale, ultimately providing a means for non-invasive, *in vivo* assessment of cell health.

Funding. National Eye Institute (EY001319, EY022371); National Science Foundation (DGE-1419118); Research to Prevent Blindness (Department of Ophthalmology, University of Rochester, Unrestricted Grant).

Acknowledgments. The authors would like to thank the following people for their contributions to this project: Qiang Yang, for development of AOSLO imaging acquisition software and firmware and image registration software, as well as assistance with implementation of fluorescence lifetime hardware; Keith Parkins, for software development for rod and cone analysis and assistance with implementation of fluorescence lifetime hardware and software; Amber Walker, Lee Anne Schery, and Louis DiVincenti, for care and handling of non-human primates and anesthesia during imaging experiments; Christina Schwarz, Robin Sharma, and Jie Zhang, for helpful advice and discussions; Jennifer Strazzeri, Brandi Hardy, and Tracy Bubel, for preparation of *ex vivo* retina; Alfredo Dubra and Kamran Ahmad, for development of adaptive optics control software; Martin Gira and Mark Ditz, for construction of the stereotaxic cart modified from a design courtesy of the US Air Force.

Disclosures. SW, JF: IDEX Health & Science (E). JJH: University of Rochester (P).

Data availability. Data underlying the results presented in this paper are not publicly available at this time but may be obtained from the authors upon reasonable request.

References

1. R. Sharma, C. Schwarz, D. R. Williams, G. Palczewska, K. Palczewski, and J. J. Hunter, "In vivo two-photon fluorescence kinetics of primate rods and cones," Invest. Ophthalmol. Vis. Sci. **57**(2), 647 (2016).
2. R. Sharma, C. Schwarz, J. J. Hunter, G. Palczewska, K. Palczewski, and D. R. Williams, "Formation and clearance of all-trans-retinol in rods investigated in the living primate eye with two-photon ophthalmoscopy," Invest. Ophthalmol. Vis. Sci. **58**(1), 604 (2017).
3. S. Walters, C. Schwarz, R. Sharma, E. A. Rossi, W. S. Fischer, D. A. DiLoreto, J. Strazzeri, D. Nelidova, B. Roska, J. J. Hunter, D. R. Williams, and W. H. Merigan, "Cellular-scale evaluation of induced photoreceptor degeneration in the living primate eye," Biomed. Opt. Express **10**(1), 66–82 (2019).
4. R. Sharma, D. R. Williams, G. Palczewska, K. Palczewski, and J. J. Hunter, "Two-photon autofluorescence imaging reveals cellular structures throughout the retina of the living primate eye," Invest. Ophthalmol. Vis. Sci. **57**(2), 632 (2016).
5. E.A. Rossi, C. E. Granger, R. Sharma, Q. Yang, K. Saito, C. Schwarz, S. Walters, K. Nozato, J. Zhang, T. Kawakami, W. Fischer, L. R. Latchney, J. J. Hunter, M. M. Chung, and D. R. Williams, "Imaging individual neurons in the retinal ganglion cell layer of the living eye," Proc. Natl. Acad. Sci. USA **114**(3), 586 (2017).
6. W. Becker, "Fluorescence lifetime imaging – techniques and applications," J. Microsc. **247**(2), 119–136 (2012).
7. D. Schweitzer, M. Hammer, F. Schweitzer, R. Anders, T. Doebbecke, S. Schenke, E. R. Gaillard, and E. R. Gaillard, "In vivo measurement of time-resolved autofluorescence at the human fundus," J Biomed Opt. **9**(6), 1214 (2004).
8. C. Dysli, G. Quellec, M. Abegg, M. N. Menke, U. Wolf-Schnurrbusch, J. Kowal, J. Blatz, O. La Schiazza, A. B. Leichtle, S. Wolf, and M. S. Zinkernagel, "Quantitative analysis of fluorescence lifetime measurements of the macula using the fluorescence lifetime imaging ophthalmoscope in healthy subjects," Invest. Ophthalmol. Vis. Sci. **55**(4), 2106 (2014).
9. M. C. Skala, K. M. Riching, A. Gendron-Fitzpatrick, J. Eickhoff, K. W. Eliceiri, J. G. White, and N. Ramanujam, "In vivo multiphoton microscopy of NADH and FAD redox states, fluorescence lifetimes, and cellular morphology in precancerous epithelia," Proc. Natl. Acad. Sci. USA **104**(49), 19494–9 (2007).

Biomedical Optics EXPRESS

10. D. Schweitzer, S. Quick, S. Schenke, M. Klemm, S. Gehlert, M. Hammer, S. Jentsch, and J. Fischer, "Vergleich von Parametern der zeitaufgelösten Autofluoreszenz bei Gesunden und Patienten mit früher AMD [Comparison of parameters of time-resolved autofluorescence between healthy subjects and patients suffering from early AMD]," Ophthalmologe **106**(8), 714 (2009).
11. C. Dysli, S. Wolf, and M. S. Zinkernagel, "Autofluorescence lifetimes in geographic atrophy in patients with age-related macular degeneration," Invest. Ophthalmol. Vis. Sci. **57**(6), 2479 (2016).
12. C. Dysli, R. Fink, S. Wolf, and M. S. Zinkernagel, "Fluorescence lifetimes of drusen in age-related macular degeneration," Invest. Ophthalmol. Vis. Sci. **58**(11), 4856 (2017).
13. L. Sauer, M. Klemm, S. Peters, D. Schweitzer, J. Schmidt, L. Kreilkamp, L. Ramm, D. Meller, and M. Hammer, "Monitoring foveal sparing in geographic atrophy with fluorescence lifetime imaging ophthalmoscopy – a novel approach," Acta Ophthalmologica. **96**(3), 257 (2018).
14. L. Sauer, R. H. Gensure, K. M. Andersen, L. Kreilkamp, G. S. Hageman, M. Hammer, and P. S. Bernstein, "Patterns of fundus autofluorescence lifetimes in eyes of individuals with nonexudative age-related macular degeneration," Invest. Ophthalmol. Vis. Sci. **59**(4), AMD65–AMD77 (2018).
15. L. Sauer, C. B. Komanski, A. S. Vitale, E. D. Hansen, and PS. Bernstein, "Fluorescence lifetime imaging ophthalmoscopy (FLIO) in eyes with pigment epithelial detachments due to age-related macular degeneration," Invest. Ophthalmol. Vis. Sci. **60**(8), 3054 (2019).
16. K. M. Andersen, L. Sauer, R. H. Gensure, M. Hammer, and P. S. Bernstein, "Characterization of retinitis pigmentosa using fluorescence lifetime imaging ophthalmoscopy (FLIO)," Trans. Vis. Sci. Tech. **7**(3), 20 (2018).
17. C. Dysli, K. Schürch, E. Pascal, S. Wolf, and M. S. Zinkernagel, "Fundus autofluorescence lifetime patterns in retinitis pigmentosa," Invest. Ophthalmol. Vis. Sci. **59**(5), 1769 (2018).
18. J. Schmidt, S. Peters, L. Sauer, D. Schweitzer, M. Klemm, R. Augsten, N. Müller, and M. Hammer, "Fundus autofluorescence lifetimes are increased in non-proliferative diabetic retinopathy," Acta Ophthalmol **95**(1), 33–40 (2017).
19. C. Dysli, S. Wolf, K. Hatz, and M. S. Zinkernagel, "Fluorescence lifetime imaging in Stargardt disease: potential marker for disease progression," Invest. Ophthalmol. Vis. Sci. **57**(3), 832 (2016).
20. Y. Solberg, C. Dysli, P. Escher, L. Berger, S. Wolf, and M. S. Zinkernagel, "Retinal flecks in stargardt disease reveal characteristic fluorescence lifetime transition over time," Retina **39**(5), 879 (2019).
21. C. Dysli, S. Wolf, H. V. Tran, and M. S. Zinkernagel, "Autofluorescence lifetimes in patients with choroideremia identify photoreceptors in areas with retinal pigment epithelium atrophy," Invest. Ophthalmol. Vis. Sci. **57**(15), 6714 (2016).
22. D. Schweitzer, M. Klemm, S. Quick, L. Deutsch, S. Jentsch, M. Hammer, J. Dawczynski, C. Kloos, and U. A. Mueller, "Detection of early metabolic alterations in the ocular fundus of diabetic patients by time-resolved autofluorescence of endogenous fluorophores," *Clinical and Biomedical Spectroscopy and Imaging II*; N. Ramanujam and J. Popp, eds., Vol. 8087 of Proceedings of SPIE-OSA Biomedical Optics (Optical Society of America, 2011), paper 80871G.
23. D. Schweitzer, L. Deutsch, M. Klemm, S. Jentsch, M. Hammer, S. Peters, J. Haueisen, U. A. Müller, and J. Dawczynski, "Fluorescence lifetime imaging ophthalmoscopy in type 2 diabetic patients who have no signs of diabetic retinopathy," J. Biomed. Opt **20**(6), 061106 (2015).
24. C. Dysli, L. Berger, S. Wolf, and M. S. Zinkernagel, "Fundus autofluorescnce lifetimes and central serous chorioretinopathy," Retina. **37**(11), 2151 (2017).
25. L. Sauer, S. Peters, J. Schmidt, D. Schweitzer, M. Klemm, L. Ramm, R. Augsten, and M. Hammer, "Monitoring macular pigment changes in macular holes using fluorescence lifetime imaging ophthalmoscopy," Acta Ophthalmol. **95**(5), 481 (2017).
26. L. Sauer, R. H. Gensure, M. Hammer, and P. S. Bernstein, "Fluorescence lifetime imaging ophthalmoscopy: a novel way to assess macular telangiectasia type 2," Ophthalmol Retina **2**(6), 587–598 (2018).
27. J. A. Feeks and J. J. Hunter, "Adaptive optics two-photon excited fluorescence lifetime imaging ophthalmoscopy of exogenous fluorophores in mice," Biomed. Opt. Express **8**(5), 2483 (2017).
28. Q. Yang, J. Zhang, K. Nozato, K. Saito, D. R. Williams, A. Roorda, and E. A, Rossi, "Closed-loop optical stabilization and digital image registration in adaptive optics scanning light ophthalmoscopy," Biomed. Opt. Express **5**(9), 3174 (2014).
29. J. I. Morgan, "In vivo imaging of the retinal pigment epithelial cells," (PhD Dissertation, University of Rochester 2008), http://hdlhandlenet/1802/5990.
30. J. R. Lakowicz, *Principles of Fluorescence Spectroscopy* (Springer Science + Business Media, 2006).
31. A. J. Walsh, J. T. Sharick, M. C. Skala, and H. T. Beier, "Temporal binning of time-correlated single photon counting data improves exponential decay fits and imaging speed," Biomed. Opt. Express **7**(4), 1385 (2016).
32. M. A. Digman, V. R. Caiolfa, M. Zamai, and E. Gratton, "The phasor approach to fluorescence lifetime imaging analysis," Biophys. J. **94**(2), L14–L6 (2008).
33. C. Stringari, A. Cinquin, O. Cinquin, M. A. Digman, P. J. Donovan, and E. Gratton, "Phasor approach to fluorescence lifetime microscopy distinguishes different metabolic states of germ cells in a live tissue," Proceedings of the National Academy of Sciences **108**(33), 13582–13587 (2011).
34. J. Zhang, R. Sabarinathan, T. Bubel, D. R. Williams, and J. J. Hunter, (eds.) "Spectral dependence of light exposeure on retinal pigment epithelium (RPE) disruption in living primate retina," IOVS 57: ARVO E Abstract 2220 (poster); 2016.

Biomedical Optics EXPRESS

35. C. Chen, E. Tsina, M. C. Cornwall, R. K. Crouch, S. Vijayaraghavan, and Y. Koutalos, "Reduction of all-trans retinal to all-trans retinol in the outer segments of frog and mouse rod photoreceptors," Biophys. J. **88**(3), 2278 (2005).
36. J. Zhang, R. Sabarinathan, T. Bubel, D. Williams, and J Hunter, (eds.) "Spectral dependence of light exposeure on retinal pigment epithelium (RPE) disruption in living primate retina," . IOVS 57: ARVO E Abstract 2220; 2016.
37. K. Chihara, T. Takemura, T. Yamaoka, N. Yamamoto, A. Schaffer, and R. S. Becker, "Visual pigments—10. Spectroscopy and photophysical dynamics of retinol and retinyl ether," Photochem Photobiol **29**(5), 1001 (1979).
38. E. R. Gaillard, S. J. Atherton, G. Eldred, and J. Dillon, "Photophysical studies on human retinal lipofuscin," Photochem Photobiol **61**(5), 448–453 (1995).
39. J. R. Lakowicz, H. Szmacinski, K. Nowaczyk, and M. L. Johnson, "Fluorescence lifetime imaging of free and protein-bound NADH," Proc. Natl. Acad. Sci. USA **89**(4), 1271 (1992).
40. R. Cubeddu, P. Taroni, D.-N. Hu, N. Sakai, K. Nakanishi, and J. E. Roberts, "Photophysical studies of A2-E, putative precursor of lipofuscin, in human retinal pigment epithelial cells," Photochem Photobiol **70**(2), 172 (1999).
41. Y. Miura, G. Huettmann, R. Orzekowsky-Schroeder, P. Steven, M. Szaszák, N. Koop, and R. Brinkmann, "Two-photon microscopy and fluorescence lifetime imaging of retinal pigment epithelial cells under oxidative stress two-photon microscopy and FLIM of RPE cells," Invest. Ophthalmol. Vis. Sci. **54**(5), 3366 (2013).
42. S. Peters, M. Hammer, and D. Schweitzer, "Two-photon excited fluorescence microscopy application for ex vivo investigation of ocular fundus samples," Proc. SPIE 8086, Advanced Microscopy Techniques II, 808605 (8 June 2011); https://doi.org/10.1117/12.889807
43. D. Schweitzer, E. R. Gaillard, J. Dillon, R. F. Mullins, S. Russell, B. Hoffmann, S. Peters, M. Hammer, and C. Biskup, "Time-resolved autofluorescence imaging of human donor retina tissue from donors with significant extramacular drusen," Invest. Ophthalmol. Vis. Sci. **53**(7), 3376 (2012).
44. G. Palczewska, M. Golczak, D. R. Williams, J. J. Hunter, and K. Palczewski, "Endogenous fluorophores enable two-photon imaging of the primate eye," Invest. Ophthalmol. Vis. Sci. **55**(7), 4438 (2014).
45. E. T. Obi-Tabot, L. M. Hanrahan, R. Cachecho, E. R. Beer, S. R. Hopkins, J. C. K. Chan, J. M. Shapiro, and W. W. LaMorte, "Changes in hepatocyte NADH fluorescence during prolonged hypoxia," Journal of Surgical Research **55**(6), 575 (1993).
46. S. Huang and A. A. Heikal, "Two-photon fluorescence spectroscopy and microscopy of NAD(P)H and flavoprotein," Biophys. J. **82**(5), 2811 (2002).
47. R. R. Birge, J. A. Bennett, B. M. Pierce, and T. M. Thomas, "Two-photon spectroscopy of the visual chromophores. Evidence for a lowest excited 1Ag–like .pi..pi.* state in all-trans-retinol (vitamin A)," J. Am. Chem. Soc. **100**(5), 1533 (1978).
48. G. I. Liou, C. D. B. Bridges, S. L. Fong, R. A. Alvarez, and F. Gonzalez-Fernandez, "Vitamin a transport between retina and pigment epithelium—an interstitial protein carrying endogenous retinol (interstitial retinol-binding protein)," Vision Research **22**(12), 1457 (1982).
49. M. A. Yaseen, J. Sutin, W. Wu, B. Fu, H. Uhlirova, A. Devor, D. A. Boas, and S. Sakadžić, "Fluorescence lifetime microscopy of NADH distinguishes alterations in cerebral metabolism in vivo," Biomed. Opt. Express **8**(5), 2368 (2017).
50. H. D. Vishwasrao, A. A. Heikal, K. A. Kasischke, and W. W. Webb, "Conformational dependence of intracellular NADH on metabolic state revealed by associated fluorescence anisotropy," J. Bio. Chem. **280**(26), 25119–26 (2005).
51. T. Tahara "Ultrafast photochemical dynamics in solution studied by femtosecond time-resolved fluorescence spectroscopy: involvement of highly excited states," Advances in Multi-Photon Processes and Spectroscopy2004. p. 1–71.
52. U. Alexiev and D. L. Farrens, "Fluorescence spectroscopy of rhodopsins: Insights and approaches," Biochimica et Biophysica Acta (BBA) - Bioenergetics **1837**(5), 694–709 (2014).
53. R. R. Birge, J. A. Bennett, L. M. Hubbard, H. L. Fang, B. M. Pierce, and DS Kliger, *et al.*, "Two-photon spectroscopy of all-trans-retinal. Nature of the low-lying singlet states," J. Am. Chem. Soc. **104**(9), 2519 (1982).
54. N. Nakashima, K. Yoshihara, F. Tanaka, and K. Yagi, "Picosecond fluorescence lifetime of the coenzyme of D-amino acid oxidase," J. Bio. Chem. **255**(11), 5261 (1980).
55. K. C. Wikler, R. W. Williams, and P. Rakic, "Photoreceptor mosaic: number and distribution of rods and cones in the rhesus monkey retina," J. Comp. Neurol. **297**(4), 499–508 (1990).
56. C. A. Curcio, K. R. Sloan, R. E. Kalina, and A. E. Hendrickson, "Human photoreceptor topography," J. Comp. Neurol. **292**(4), 497–523 (1990).
57. O. Packer, A. E. Hendrickson, and C. A. Curcio, "Photoreceptor topography of the retina in the adult pigtail macaque (Macaca nemestrina)," J. Comp. Neurol. **288**(1), 165 (1989).
58. C. A. Curcio, K. R. Sloan, O. Packer, A. E. Hendrickson, and R. E. Kalina, "Distribution of cones in human and monkey retina: individual variability and radial asymmetry," Science **236**(4801), 579–582 (1987).
59. A. E. Elsner, S. A. Burns, and R. H. Webb, "Mapping cone photopigment optical density," J. Opt. Soc. Am. A **10**(1), 52 (1993).
60. D. M. Snodderly, M. M. Sandstrom, I. Y-F. Leung, C. L. Zucker, and M. Neuringer, "Retinal pigment epithelial cell distribution in central retina of rhesus monkeys," Invest. Ophthalmol. Vis. Sci. **43**(9), 2815 (2002).
61. L. Sauer, D. Schweitzer, L. Ramm, R. Augsten, M. Hammer, and S. Peters, "Impact of macular pigment on fundus autofluorescence lifetimes," Invest. Ophthalmol. Vis. Sci. **56**(8), 4668 (2015).

Biomedical Optics EXPRESS

62. D. Schweitzer, S. Schenke, M. Hammer, F. Schweitzer, S. Jentsch, and E. Birckner, *et al.*, "Towards metabolic mapping of the human retina," Microsc. Res. Tech. **70**(5), 410 (2007).
63. M. Hammer, L. Sauer, M. Klemm, S. Peters, R. Schultz, and J. Haueisen, "Fundus autofluorescence beyond lipofuscin: lesson learned from ex vivo fluorescence lifetime imaging in porcine eyes," Biomed. Opt. Express **9**(7), 3078 (2018).
64. F. C. Delori, C. K. Dorey, G. Staurenghi, O. Arend, D. G. Goger, and J. J. Weiter, "In vivo fluorescence of the ocular fundus exhibits retinal pigment epithelium lipofuscin characteristics," Invest. Ophthalmol. Vis. Sci. **36**(3), 718 (1995).
65. G. E. Eldred and M. L. Katz, "Fluorophores of the human retinal pigment epithelium: Separation and spectral characterization," Experimental Eye Research **47**(1), 71–86 (1988).
66. F. Docchio, M. Boulton, R. Cubeddu, R. Ramponi, and P. D. Barker, "Age-related changes in the fluorescence of melanin and lipofuscin granules of the retinal pigment epithelium: a time-resolved fluorescence spectroscopy study," Photochem Photobiol **54**(2), 247 (1991).
67. C. N. Keilhauer and Delori. F. o. C., "Near-infrared autofluorescence imaging of the fundus: visualization of ocular melanin," Invest. Ophthalmol. Vis. Sci. **47**(8), 3556 (2006).
68. C. E. Granger, Q. Yang, H. Song, K. Saito, K. Nozato, and L. R. Latchney, *et al.*, "Human retinal pigment epithelium: in vivo cell morphometry, multispectral autofluorescence, and relationship to cone mosaicin vivo rpe cell morphometry," Invest. Ophthalmol. Vis. Sci. **59**(15), 5705 (2018).
69. L. Sauer, K. M. Andersen, B. Li, R. H. Gensure, M. Hammer, and P. S. Bernstein, "Fluorescence lifetime imaging ophthalmoscopy (FLIO) of Macular Pigment FLIO of macular pigment," Invest. Ophthalmol. Vis. Sci. **59**(7), 3094 (2018).
70. D. M. Niedzwiedzki, J. O. Sullivan, T. Polívka, R. R. Birge, and H. A. Frank, "Femtosecond time-resolved transient absorption spectroscopy of xanthophylls," J. Phys. Chem. B **110**(45), 22872–85 (2006).
71. F. C. Delori, D. G. Goger, B. R. Hammond, D. M. Snodderly, and S. A. Burns, "Macular pigment density measured by autofluorescence spectrometry: comparison with reflectometry and heterochromatic flicker photometry," J. Opt. Soc. Am. A **18**(6), 1212 (2001).
72. C. Schwarz, R. Sharma, S. K. Cheong, M. Keller, D. R. Williams, and J. J. Hunter, "Selective S cone damage and retinal remodeling following intense ultrashort pulse laser exposures in the near-infrared," Invest. Ophthalmol. Visual Sci. **59**(15), 5973–5984 (2018).
73. C. Schwarz, R. Sharma, W. S. Fischer, M. Chung, G. Palczewska, K. Palczewski, D. R. Williams, and J. J. Hunter, "Safety assessment in macaques of light exposures for functional two-photon ophthalmoscopy in humans," Biomed. Opt. Express **7**(12), 5148–5169 (2016).
74. G. Palczewska, J. Boguslawski, P. Stremplewski, L. Kornaszewski, J. Zhang, and Z. Dong, *et al.*, "Noninvasive two-photon optical biopsy of retinal fluorophores," Proc. Natl. Acad. Sci. USA **117**(36), 22532–22543 (2020)..
75. M. A. Feldman, T. B. Arbukhanova, P. M. Borzenok, S. A. Kuzmin, V. A. Ostrovsky, and M. A. , "Estimation of fluorescence lifetime of lipofuscin fluorophores contained in lipofuscin granules of retinal pigment epithelium of human cadaver eyes without signs of pathology," Dokl Biochem Biophys **472**(1), 19–22 (2017).
76. S. He, C Ye, Q. Sun, C. K. S. Leung, and J. Y. Qu, "Label-free nonlinear optical imaging of mouse retina," Biomed. Opt. Express **6**(3), 1055–1066 (2015).